

Stress maximization of mono crystalline silicon cantilever blades

Bachelor Thesis

J.G.N. Geurtsen

Student number:
09067922

May 30, 2013



National institute for subatomic physics, Nikhef
Amsterdam

DE HAAGSE
HOGESCHOOL

The Hague University
Delft

First Internship coach: mvr. drs. M.C. Vloemans
Second Internship coach: dhr. dr. L.H. Arntzen
Company mentor: dhr. ir. E. Hennes

Preface and acknowledgment

The Hague university demands an internship of seventeen weeks for a bachelor degree in applied physics. I am glad the dutch institute Nikhef wanted an intern and gave me this opportunity. During this internship I learned a lot and I would like to thank E. Hennes for the help with theoretical problems. Further I want to thank M. Doets for designing my experimental setup and M. Jaspers for building the device. A. Bertolini for helping with the physics in general. Also a compliment to J. Rovenkamp who has cut all the hand-cut blades what he has done perfectly. A special thanks to F. Schimmel who implemented all the data acquisition devices and made the LabVIEW program. And finally of course everyone for the collegiality.

Abstract

A new gravitation wave observatory is being built in Japan. This facility is a big Michelson interferometer where the mirrors and sensors will be made cryogenic down to 4 K. The problem is that: the heat cannot be transported out of the mirror by its surroundings because the whole system is in an ultra-high vacuum. Also a fraction of the LASER power, in the order of 2 W, will be stored in the mirror. This heat can only be transported using the suspension of the mirror. To transport this heat, the wires of the mirror can be made real thick. But now the suspension will be too stiff which decreases the vibration noise properties. It will also still take up to one year before the mirrors reach a temperature of 4 K. For a good transportation of the heat, the idea is that: thick sapphire wires will be used to hang the mirror and for good vibration properties silicon cantilevers will hang the mirror with a low vibration frequency. The bending performance of silicon cantilevers depends highly on the surface conditions because silicon is a brittle material.

The goal of this research is finding the best cantilever blade condition which insures good bending performance. The bending performance depends on several surface conditions. The surface needs to be smooth and without cracks. These cracks cause weak spots in the cantilever. To minimize the cracks several cutting methods are performed, namely: cutting by hand, machine-cutting and High Reactive ion etching. Chemical etching of the edges is used as an after-cut-treatment in attempt to minimize the cracks.

To measure the stress at a certain point of the blade an experimental setup has been made. This setup can compress a blade till it buckles and eventually breaks. The compression distance Δx , the compression force F_x , the tip angle θ and the height of the blade center h can be measured. Using these quantities, the stress σ at the surface of the blade can be calculated. The compression distance will be made larger in small steps till the blade breaks. The measurement right before the blade breaks will be used to calculate the stress.

A numerical analysis has been made to support the measurements. This analysis delivers the expected blade shape at any state of bending. Note that this does not predict the breaking of the blade. The forces and stresses in the blade can also be predicted if the E-modulus is known.

The first measurements have been performed with a diamond knife-cut edge. This is done by hand using a protractor and a diamond knife. The average maximum feasible stress is 280 MPa. This blade does have a large breaking bandwidth with a standard deviation is 130 MPa. Big cracks at the edge of the blade ensures weak spots. These weak spots are unwanted, therefore a different solution had to be found.

The second set of measurements are also performed with a diamond knife only now, a cutting machine is used. The cut is made parallel to the (110)-crystal plane orientation. The average maximum stress the blades can manage right before it breaks is: 530 MPa which is higher than the hand cut blades and the standard deviation of: 40 MPa is smaller than that of the hand-cut measurements. However, the blades are less strong if the blades are not cut straight parallel to a crystal plane. With an estimated error of 5% to the (110)-plane, the average stress is 200 MPa and the standard deviation is 50MPa. This shows the importance of cutting along a crystal plane.

The third set of measurements are performed with Deep Reactive Ion Etching. Now, the average maximum bending stress is 270 MPa with a standard deviation of 50 MPa. The breaking bandwidth is smaller than that of the hand-cut blades because the blade edges are much smoother. The maximum feasible stress is not that high as the blades cut with the cut-machine probably because of micro cracks and internal stresses within the blade.

The fourth measurement are hand-cut blades. Only now the edges are sandpapered and chemical etched in KOH. The average maximum stress is now: 200 MPa. This method makes the blades worse than the hand-cut blades and this is not a good blade optimization method.

Contents

1	Introduction	1
2	Application	2
3	Physics of stress and bending	5
3.1	Material properties	5
3.2	Chemical etching	7
3.3	Measuring the stress	8
3.4	Blade bending analysis	10
3.5	Numerical analysis	12
4	Experimental setup	15
4.1	Calibration of the rotation sensor	16
4.2	Calibration of the load sensors.	19
5	Stress measurement results	22
5.1	Hand-cut blades	22
5.2	Machine-cut blades	23
5.3	Deep reactive ion etched blades (DRIE)	25
5.4	Chemical etched cantilevers	26
6	Conclusion and discussion	29
7	Bibliography	30
A	Werkplan	31
B	Derivation of the second moment of area	32
C	Derivation of the dimensionless differential equation.	33

1 Introduction

A new facility is under construction named "KAGRA" in Japan. This facility will be made cryogenic down to 4 K. silicon cantilevers and sapphire wires are needed to reach this temperature and stay at this temperature. If the temperature of the mirror is 4 K, the mirror needs to stay at this temperature even when a high powered LASER will be storing a fraction of its energy in the mirror. If the suspension wires will be made a lot thicker (in order of 1000 times) the wires will be too stiff to insure good vibration noise properties. This is why the thick wires are applied to cantilevers. If the old material will be used, it still will take too long before the mirror is cooled down. Therefore the cantilevers will be made of silicon and the wires of sapphire. This will insure good heat transportation. The goal of this internship is finding the best silicon cantilever condition which insures good bending performance. More about the application will be explained in chapter 2.

The flexures are rectangular in shape and are cut or etched out of a thin (0.2 - 0.4 mm) polished commercial wafer. An experimental setup is prepared at Nikhef to measure the stress. This setup measures the compression distance, compression force, height of the flexure, and the rotation angle at the end of the flexure as shown in figure 1. With these known parameters, the bending stress can be calculated. This answer will be checked with a numerical analysis made in Excel. The research will be focused on finding conditions giving the maximum feasible stress of mono-crystalline silicon flexures. For the optimization of the flexures several methods will be used. The expectation is that the weakest point of the flexures are on the edges, because only the edges are not etched or polished. To maximize the breaking stress, the edges will be optimized which are cut under several conditions. This is done with a chemical etch method, Deep Reactive Ion Etching, and machine-cutting.

In short: This thesis includes the understanding of the background physics of bending and analyzing and simulating of the stress of the silicon flexures (Chapter 3). Also the experimental setup (described in chapter 4) is calibrated. The original job description can be read in appendix A.

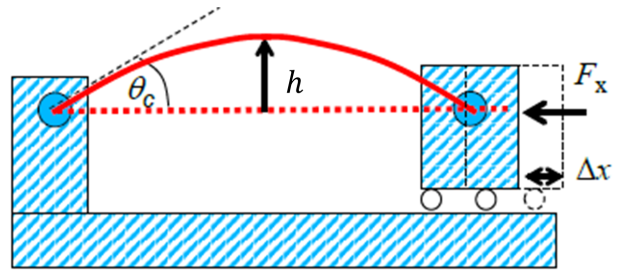


Figure 1: Picture of the experimental setup.

2 Application

The general relativity theory of Albert Einstein predicted in 1916 how gravitational waves cause fluctuations in the space-time dimensions. These gravitational waves traveling outward from the source with the speed of light. These fluctuations cause, when arriving on earth, a length change of everything. This gravitational waves are hard to measure because the objects with the largest share of source, such as: white dwarfs, black holes and neutron stars are far away from the earth. The energy expands in a sphere with:

$$h = \frac{1}{r^2} \quad (1)$$

Where h is the amplitude of the wave and r is the distance between object and earth. This is

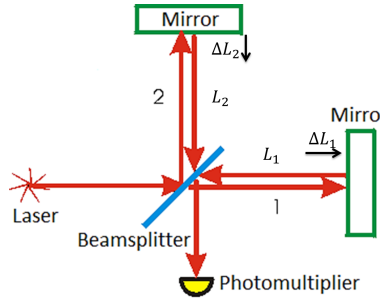


Figure 2: Schematic illustration of a Michelson interferometer.

why almost all the gravitational wave energy will not arrive on earth. Physics theorists calculated that typical strains $\frac{\Delta L}{L}$ which has to be measured on earth are in the order of 10^{-22} . Gravitational waves can be measured with a big Michelson interferometer. A Michelson interferometer uses the interference pattern of light to determine a length change as shown in figure: 2. The bigger the arms of the interferometer are, the smaller length fluctuations can be measured which can be explained with: $\Delta L = hL$. If the interferometer is set such a way that the interference of the light is destructive, an ultra sensitive photomultiplier can be used to measure small length changes[1].

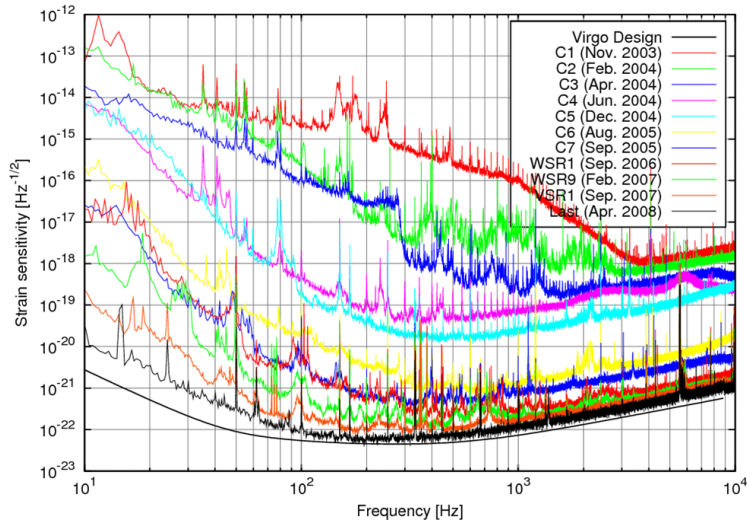


Figure 3: The strain sensitivity of Virgo from 2003 till 2008[2].

The facilities in use are called Virgo, GEO and Ligo. Virgo is the European Gravitational Observatory (EGO). The Germans have an own facility called GEO and Ligo is the American gravitational wave detector. These detectors are big Michelson interferometers. Virgo has two arms with a length of 3 km each, where Ligo has two arms of 4 km each. Because of multiple reflections in the arms, Virgo has a effective arm length up to 120 kilometers. To avoid motions of all the components, every component is isolated by a 10 meter high system of pendulums. The hole system operates in an ultra high vacuum to prevent distortion by colliding gases molecules. The environment of the Virgo Interferometer is quieter than that of a spacecraft orbiting around the earth[1]. Also Ligo and Virgo are the largest ultra high vacuum vessels in the world[1]. Theoretically with the sensitivity of Virgo nowadays, the detector should measure a gravitational wave once a year. This is why there are plans to built new better facilities. As shown in figure 3, the design sensitivity of Virgo was almost reached in 2008. At this moment The Virgo and Ligo facilities are being upgraded called advanced Virgo and advanced Ligo. This research is performed for new facilities which are being built in the mountains

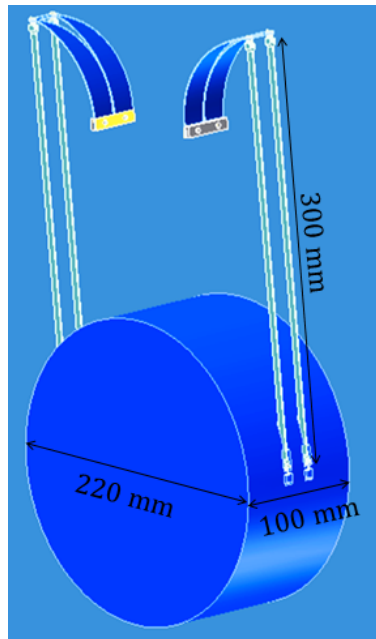


Figure 4: The application setup. The cantilevers are made of silicon and the wires and the mirror of sapphire[2].

of Japan called 'KAGRA' and the European version 'ET' which will be constructed in approximately 2025. These facilities will be built underground to reduce the seismic noise. Also the used mirrors will be cryogenic down to 4 K which will reduce the thermal noise. Theoretically, a strain sensitivity of approximately $10^{-24} \text{ Hz}^{-1/2}$ will be reached with these changes[2]. In these facilities the mirrors of the Michelson-interferometer would not only be in an ultra high vacuum, but needs also to cool down to 4 K. The heat cannot be transported good enough because the mirrors are in a ultra high vacuum and the attachments do not conduct the heat quick enough at these low temperatures. The LASER also store warmth into the mirror. Now several problems will occur with the setup. To drain the heat as shown in figure 4, the wires can be made a lot thicker. The wires will be 2 cm thick instead of $50 \mu\text{m}$. And the wires are mounted on cantilevers. This is done because of the big stiffness of the wires. The stiffness needs to be almost zero for good noise properties of the setup. Unfortunately it still can take up to one year before the mirrors are at a temperature of 4 K. Therefor mono crystalline silicon cantilevers and sapphire (Al_2O_3) wires will be used. This material conducts enough heat for a quick

cool-down of the mirrors. In figure 5 the heat conductivity of silicon, sapphire and silica(glass) as a function of temperature are shown. The heat conductivity of silicon is hundred times higher than that of silica[2].

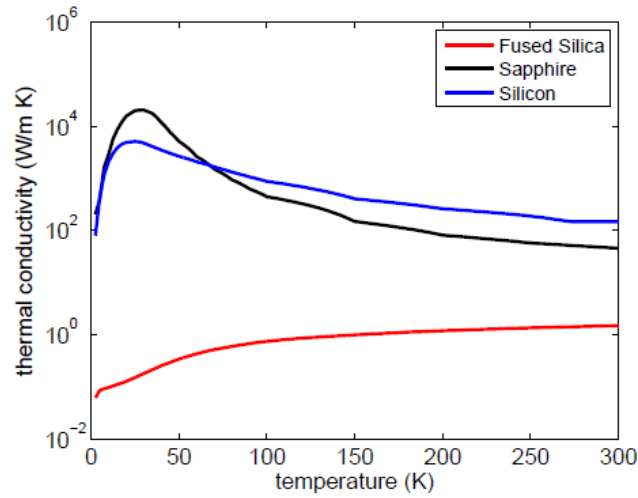


Figure 5: Thermal conductivity of silica, silicon and sapphire versus the temperature[2].

Thick sapphire wires and thin cantilevers of silicon are used to ensure the flexibility of the system. This will hang the mirror free from noise and it also ensures good heat transportation. The flexures are mounted in clamps. Between the clamps and the flexures, thin Indium foil is applied. Indium foil ensures the blades from breaking in the clamp because silicon and sapphire are brittle materials. The cantilever blades will be triangular. This is because of the stress spreading as a function of the length. This flexures will be optimized to manage as much tensile stress as possible. The prediction is that the weakness of a silicon blade is caused by the edges. The edges of the silicon blades are cut out of a big wafer. The blade will break at the point where already small cracks are. The size of these cracks can be manipulated by the way of cutting and after-cut-treatments. Several ways of optimization will be examined by simply perform different cuts and treatments. With these different samples the maximum experienced stress of the cantilever blade can be measured. In this research, the focus will be on testing and optimizing rectangular silicon flexures. rectangular blades are used facilitate the material properties testing.

3 Physics of stress and bending

This chapter will explain the physics behind bending. First important equations are shown and some material properties will be described[3]. The quantities that will be used for measuring the stress will be derived. Also the physical explanation of the numerical analysis and the description of the blade curve will be explicated in this chapter.

3.1 Material properties

When a force is applied to a sample, as is shown in figure 6. The length of a sample will change as[3]:

$$L_0 \rightarrow L_0 + \Delta L \quad (2)$$

where:

$$\begin{aligned} L_0 &= \text{Length of the sample at rest} && [-] \\ \Delta L &= \text{Length change of the sample} && [\text{m}] \end{aligned}$$

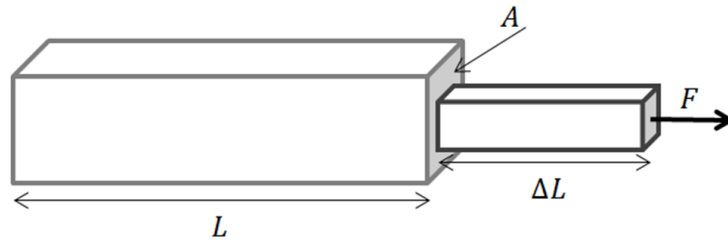


Figure 6: Visual illustration of a typical deformation of a sample caused by stretching a beam.

Strain is a normalized measure of deformation which is only valid within the strain limit. The Strain is given by:

$$\varepsilon_x = \frac{\Delta L_x}{L_x} \quad (3)$$

where:

$$\begin{aligned} \varepsilon_x &= \text{strain} && [-] \\ L_x &= \text{length of the sample} && [\text{m}] \end{aligned}$$

Note that ΔL can be negative which impact that the sample will be compressed. It is clear that the bigger a cross section surface of a sample is, the more force is needed to strain a sample by ε_x . The force per unit area is called the stress and is given by:

$$\sigma = \frac{F}{A} \quad (4)$$

where:

$$\begin{aligned} \sigma &= \text{stress} && [\text{Pa}] \\ F &= \text{force} && [\text{N}] \\ A &= \text{cross section surface} && [\text{m}^2] \end{aligned}$$

Hooke's law states that a stressed sample will deform elastically, the stress is proportional to the strain. Hooke's law is given by:

$$\sigma = E\varepsilon \tag{5}$$

where:

E =Young's modulus

The Young's modulus also called the elasticity modulus, is a result of the inter-atomic forces between the constituent atoms. Crystalline silicon has a symmetry of a cubic structure. The magnitude of Young's modulus depends on the orientation of the crystal structure. As shown in figure 7 the E-modulus has a variation of 30% between the (110)-plane and (100)-plane direction. If the silicon wafer is doped with a certain amount of chemical impurities the elasticity properties do not change much. The changes in elasticity are typically between the 1%-3% compared with non-doped silicon.[4]

Crystalline silicon will be used as cantilever. When the blade bends, in the upper surface a tensile stress will occur and in the bottom-surface a compressive stress will occur. This is illustrated in figure 8. Silicon is a brittle material, which means the material only stretch elastically until failure. This means that there will not be any plastic deformation because the sample will burst at some point.

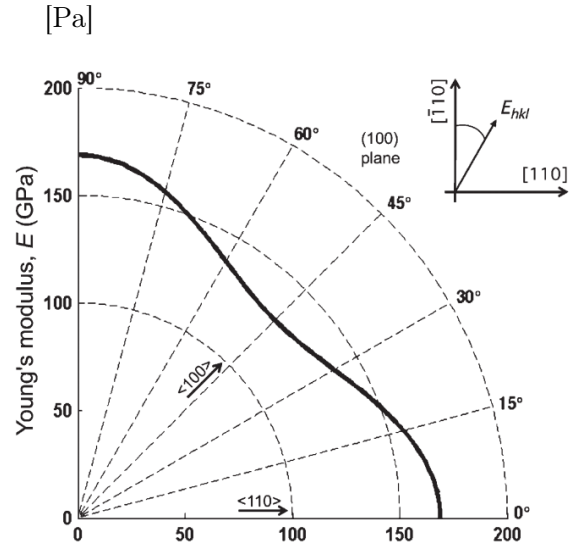


Figure 7: The Young's modulus as a function of the orientation[4].

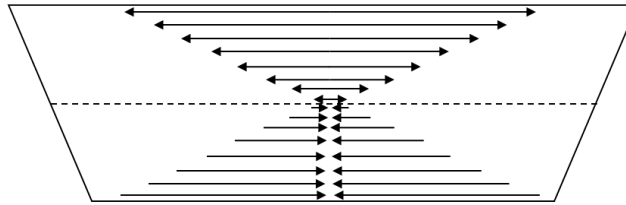


Figure 8: a schematic illustration of the stress at certain points .

The Ultimate Tensile Stress (UTS) is smaller than the Ultimate Compression Stress (UCS). This means that when a tensile stress is applied, the sample will break at a lower absolute stress than when a compression stress is applied. This is called crack growth[5]. Micro cracks are little bursts in the surface of a sample. This burst will be larger if a tensile stress is applied. This is shown in figure 9. The weakest point is where a small crack are positioned. The Young's modulus in the surface will

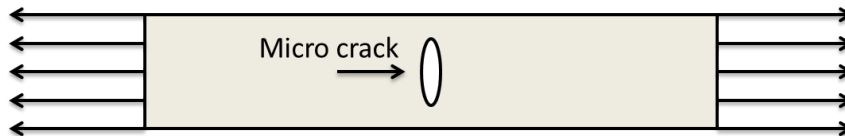


Figure 9: Schematic reproduction of a grown micro crack caused by tensile stress.

be smaller during tensile stress if a bigger amount of these micro cracks are positioned in the surface.

Also the size of these cracks does have an influence at the strength. This also shows that the UTS is smaller than the UCS which is schematically shown in figure: 10. Micro cracks can be minimized

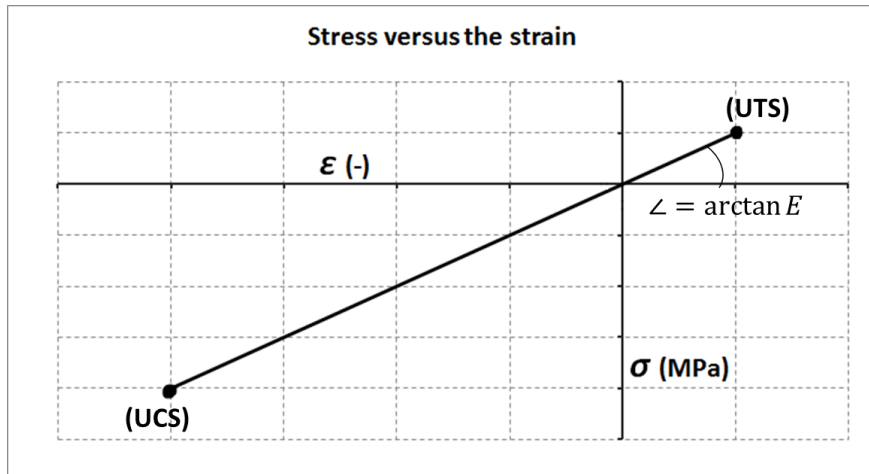


Figure 10: Schematic reproduction of the stress versus the strain of a brittle material.

using serious polishing or chemical etching. Because most of the cracks are expected to be in the edges, edge optimization is will be done.

3.2 Chemical etching

Chemical etching will be used as after-cut-treatment in a try to improve the smoothness of the blade edge. This Chemical etch will be performed with potassium hydroxide (KOH). 20 wt% KOH will be mixed with 80 wt% water (H_2O). The etch rate of the KOH depends on the percentage KOH in water and the temperature. The equation for the etch rate can be estimated with[6]:

$$R_{100} = 2.6 \cdot 10^6 \cdot m^{2.5} \cdot e^{-\frac{m}{300} + 0.48}{k \cdot T} \quad (6)$$

where:

R_{100} = etch rate in the (100)-plane direction	$[\mu\text{m/h}]$
m = weight percentage of KOH in water	$[-]$
k = Boltzman constant	$[8.617 \cdot 10^{-5} \text{ eV/K}]$
T = temperature	$[K]$

Note that this etch rate can vary a lot. This equation can be used as indication to the etch rate of a (100)-plane silicon wafer. Shown in figure 11, only the edge of the blade will be in the etchant. This ensures no thickness loss at the center and only the edge will be etched.

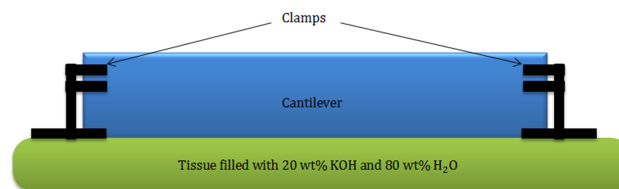


Figure 11: Visual illustration the etch setup.

3.3 Measuring the stress

The stress cannot be measured directly. Therefore a derivation for the moment will be used. The moment for a rectangular cantilever is given by (for derivation see appendix B):

$$M = \frac{EI}{R} = \frac{E wt^3}{R 12} \quad (7)$$

where:

w = width	[m]
t = thickness	[m]
I =second moment of area	[m ⁴]
R = radius of curvature	[m]
M =Moment	[Nm]

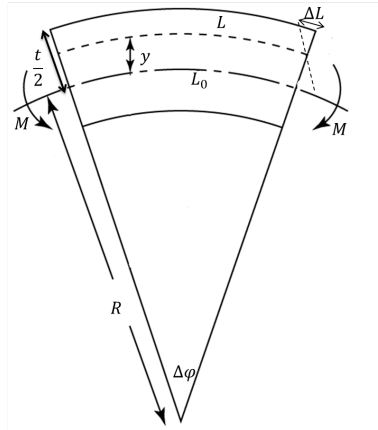


Figure 12: Schematic illustration of a small piece of blade.

ΔL is the extra length at the top of the blade caused by bending, as illustrated in figure 12. The extra length at the surface of the blade while bending can be described like:

$$L = L_0 + \Delta L \quad (8)$$

The curvature is a measure of an object which distinct the object from being flat and can be written as:

$$\kappa = \frac{1}{R} = \varphi' = \frac{d\varphi}{dL} \approx \frac{\Delta\varphi}{L_0} \quad (9)$$

where:

κ = curvature	[m ⁻¹]
φ' =derivative angle	[rad]

$\frac{\Delta\varphi}{L_0}$ is only valid when $L_0 \ll R$. Also the curvature is known which means the length change ΔL can be calculated with:

$$L = \varphi(R + \frac{t}{2}) \quad (10)$$

$$L_0 = \varphi R \quad (11)$$

Subtracting equation (11) from (10) gives:

$$\Delta L = \varphi \frac{t}{2} \quad (12)$$

Now, the strain at the top of the beam will be:

$$\varepsilon = \frac{\Delta L}{L_0} = \frac{\varphi t}{2L_0} = \frac{t}{2R} \quad (13)$$

With the strain and the Youngs modulus, the stress at the top of the blade can be calculated.

$$\sigma = E\varepsilon = \frac{Et}{2R} \quad (14)$$

Using equation 7 the equation above can be written like:

$$\sigma = \frac{EMt}{2EI} = \frac{Mt}{2I} \quad (15)$$

As shown in equation 15, the stress can be calculated without using the E-modulus. The moment can also be written as force times arm which is:

$$M = F_x \times h \quad (16)$$

where:

h = height at the center of the blade [m]
 F_x = measured force in the x direction [N]

The total height at the center of the blade can be used because this vector is perpendicular to the force vector. This equation will be used for calculating the stress. The equation becomes:

$$\sigma = \frac{F_x h t}{2I} \quad (17)$$

The blade will not always break exactly in the middle because the breaking point of the cantilever depends on the smoothness of the edge. This means that the stress at the point of breaking is not the calculated maximum stress in the middle of the blade but possibly a lower stress at a certain point on the cantilever. Unfortunately the cantilever does not always break in two pieces but often a various pieces, which means that the breaking point can not always be identified. Therefore only the stress at the middle of the cantilever will be calculated. This will be eventually a measure of the strength of a blade.

3.4 Blade bending analysis

The principle of the bending moment can be described as in figure 13. Because of its symmetry, only half the blade is needed to describe the total blade. Note that the displacement in the x-direction is now only half the displacement compared with the cantilever in reality. The equation for the bending moment can be described on the basis of figure 13. Eventually the derived equation will be used for the numerical analysis, which is described in chapter 3.5. The total equation for the bending moment of a uniform flexure is in general:

$$M(l) = -F_x(z_L - z_l) + F_z(x_L - x_l) + M \quad (18)$$

where

F_x =external horizontal force

F_z =external vertical force

z_l =the height of the blade at point l

x_l =the horizontal position at point l

M = external moment

[N]

[N]

[m]

[m]

[Nm]

F_z is zero because there is no weight hanging at the tip of the blade and the external moment is zero because the tip can rotate freely. Now the bending moment can be written as:

$$M(l) = -F_x(z_L - z_l) \quad (19)$$

Combining equation 9 and 7 shows that $M(l)$ can also be written as:

$$M(l) = \kappa EI = EI \frac{d\varphi}{dl} \quad (20)$$

combining 19 and 20 gives the differential equation for φ

$$EI \frac{d\varphi}{dl} = -F_x(z_L - z_l) \quad (21)$$

For a little displacement, $z(l) \ll L$ can be written $\sin \varphi = \varphi$. Which gives:

$$\frac{d\varphi}{dl} \approx \frac{d^2z}{dl^2} \quad (22)$$

Equation 21 can now be written as:

$$EI \frac{d^2z}{dl^2} = -F_x(z_L - z_l) \quad (23)$$

To solve differential equation 23 it is convenient to differentiate again.

$$\frac{d^3z}{dl^3} = -\frac{F_x}{EI} \frac{dz}{dl} \quad (24)$$

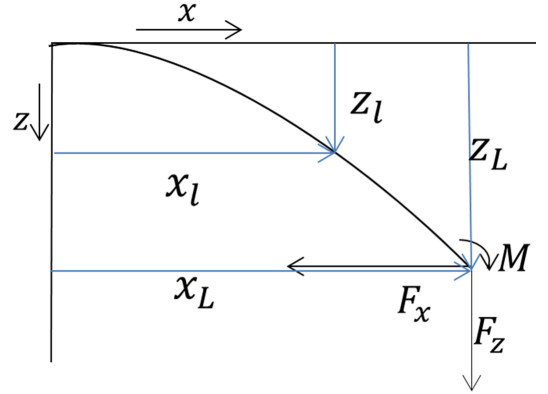


Figure 13: Schematic illustration of a blade that bends.

The differential equation can be solved with $\alpha^2 = \frac{F_x}{EI}$,

$$z(l)''' = -\alpha^2 z' \quad (25)$$

Set $z(l)' = q(l)$ then:

$$q(l)'' = -\alpha^2 q(l) \quad (26)$$

The only function where the second derivative is minus the same function are the sine and cosine functions. Therefore can be written:

$$q(l) = z'(l) = c_1 \cos(\alpha l) + c_2 \sin(\alpha l) \quad (27)$$

Integration of this function gives:

$$z(l) = A + B \sin \alpha l + C \cos \alpha l \quad (28)$$

A, B and C will be solved with the known preconditions:

$$z(0) = 0, \quad z'(0) = 0, \quad z''(L) = 0 \quad (29)$$

Where $z''(L) = 0$ because of zero moment in point L. Substituting equations 29 into 28 gives:

$$C = -A, \quad 0 = B, \quad 0 = -B\alpha^2 \sin \alpha L - C\alpha^2 \cos \alpha L \quad (30)$$

This gives:

$$0 = -A\alpha^2 \cos \alpha L \quad (31)$$

Equation 31 is trivial. If A is chosen to be 0 the blade does not bend at all. This means $\cos \alpha L$ needs to be set to zero. Which means:

$$\alpha L = \frac{\pi}{2} \quad (32)$$

This means, the blade buckles in a half sine form. Now the α can be written with two different equations:

$$\alpha = \frac{\pi}{2L} = \sqrt{\frac{EI}{F}} \quad (33)$$

This is proof of the presence of buckling force. The buckling force is the force that is needed to buckle a beam or blade. The buckling force has the largest share of force. A small variation of force is needed to buckle a beam more or less after the buckling force is reached. Where $\frac{\pi}{2L}$ means that the blade will buckle in a half sine wave form. The buckling force can be described like:

$$\frac{\pi^2}{4L^2} = \frac{F_x}{EI} \rightarrow F_b = \frac{\pi^2 EI}{4L^2} \quad (34)$$

This is the same of the buckling force which can be found in the literature. The buckling force is given by[7]:

$$F_b = \frac{m^2 \pi^2 EI}{(KL)^2} \quad (35)$$

where:

F_b = critical buckling force	[N]
m = number of half sinus waves	[-]
L = effective length of the blade	[m]
K = effective length factor	[2,0]

The curvature which describes the total blade can be derived using equation 28 and $C = -A$ and $B = 0$. With this given the next equation can be written:

$$z = A(1 - \cos \alpha L) \quad (36)$$

Because A is the amplitude, equation 36 can be written as:

$$z = z_L(1 - \cos \alpha L) \quad (37)$$

This equation describes the total blade curvature.

3.5 Numerical analysis

A Numerical analysis uses a differential equation to approach the curvature of the blade. This approach can be as accurate as needed by changing the step size. A numerical analysis can be made by using differential equation 38:

$$\frac{d^2\varphi}{dl^2} = -\frac{F_x}{EI} \frac{dz}{dl} \quad (38)$$

Using the rules of goniometry:

$$\frac{dz}{dl} = \sin(\varphi) \quad (39)$$

With equation 38 and 39 the differential equation can be written as:

$$\frac{d^2\varphi}{dl^2} = -\frac{F_x}{EI} \sin \varphi \quad (40)$$

This differential equation can be made valid for every thickness, length, width and positions of the blade, if every quantity is normalized. The dimensions can be filled in at the end of the calculations. Now, a specific answer will be achieved. For dimensionless equations the quantities can be normalized like:

$$\Gamma = \frac{l}{L_0} \quad (41)$$

$$X = \frac{x}{L_0} \quad (42)$$

$$Z = \frac{z}{L_0} \quad (43)$$

$$\omega = \frac{w}{L_0} \quad (44)$$

$$G_x = \frac{12L_0^2 F_x}{EI} \quad (45)$$

$$\phi = \frac{d\varphi}{dl} L_0 \quad (46)$$

where:

Γ = normalized length of the blade

X = normalized horizontal position

Z = normalized vertical position

ω = normalized width of the blade

[-]

[-]

[-]

[-]

ϕ =normalized first derivative angle

[rad]

Now, the differential equation becomes as derived in appendix C:

$$\frac{d^2\phi}{d\Gamma^2} = -G_x \sin \phi \quad (47)$$

Also is known:

$$\frac{dX}{d\Gamma} = \cos \phi \quad (48)$$

$$\frac{dZ}{d\Gamma} = \sin \phi \quad (49)$$

With the preconditions that: $X(0) = 0$, $Z(0) = 0$ and $\varphi(0) = 0$, the Differential equations can be solved using numerical analysis in Microsoft Excel. The numerical analysis with dimensionless quantities is helpful because this describes a general function of the blade and is general valid for rectangle blades. This gives the opportunity to approximate differential equation 47 with the solver function. This function can vary the trail values in such a way that the input values are the known values of the user[8]. The differential equation is given by:

$$\frac{d^2\phi}{d\Gamma^2} \rightarrow \phi'' = -G_x \sin \phi \quad (50)$$

In which the G_x is the normalized force. To solve this in excel several Euler steps are required.

$$\Gamma_i = \frac{i}{N} \quad (51)$$

$$\phi = \phi_{i-1} + \phi'_{i-1}(\text{d}\Gamma) \quad (52)$$

$$\phi' = \phi'_{i-1} + \phi''_{i-1}(\text{d}\Gamma) \quad (53)$$

$$X_i = X_{i-1} + \text{d}\Gamma \cos \phi_i \quad (54)$$

$$Z_i = Z_{i-1} + \text{d}\Gamma \sin \phi_i \quad (55)$$

where

i = Euler step (0,1...N)

[-]

N =total number of Euler steps

[-]

With this equations given, the Z coordinates and the G_x can be calculated by a given $X_{Ntarget}$. The $X_{Ntarget}$ is the value of the displacement ΔX applied by the force G_x . The first three steps of the excel calculation is given in table 1.

Table 1: The first three step functions used in Excel.

$\Gamma(-)$	$\phi(\text{rad})$	$\phi'(\text{rad})$	$\phi''(\text{rad})$	$X(-)$	$Z(-)$
0	$\phi_0=0$	$\phi'_0 = \phi'_{trial}$	$-G_{xtrial} \sin \phi_0$	$X_0 = 0$	$Z_0 = 0$
$\frac{1}{N}$	$\phi_1 = \phi_0 + \phi'_0 \text{d}\Gamma$	$\phi'_1 = \phi'_0 + \phi''_0 \text{d}\Gamma$	$-G_{xtrial} \sin \phi_1$	$X_1 = X_0 + \text{d}\Gamma \cos \varphi$	$Z_1 = Z_0 + \text{d}\Gamma \sin \varphi$
$\frac{2}{N}$	$\phi_2 = \phi_1 + \phi'_1 \text{d}\Gamma$	$\phi'_2 = \phi'_1 + \phi''_1 \text{d}\Gamma$	$-G_{xtrial} \sin \phi_2$	$X_2 = X_1 + \text{d}\Gamma \sin \varphi$	$Z_2 = Z_1 + \text{d}\Gamma \sin \varphi$

By changing the variables ϕ'_{trial} and G_{xtrial} and setting the known values: ϕ'_N , and $L - X_{NTarget}$ to zero, the blade can be solved iterative using the solver function. This function will change ϕ'_{trial} and G_{xtrial} in such a way the known values will be zero.

Now, the Numerical analysis will be checked for reliability. Measurements are performed with a copper beryllium blade. This blade will be compressed from 0 mm to 2 mm. Between this parameters, the center of the blade will be at a certain height. This height will be compared with the Numerical analysis. The parameters of the copper beryllium blade are:

Length: 70 ± 1 mm
 Width: 10.0 ± 0.5 mm
 Thickness: 255 ± 5 μm
 E-Modulus: 124 ± 10 GPa [9]

The height versus the compression displacement is given in figure 14.

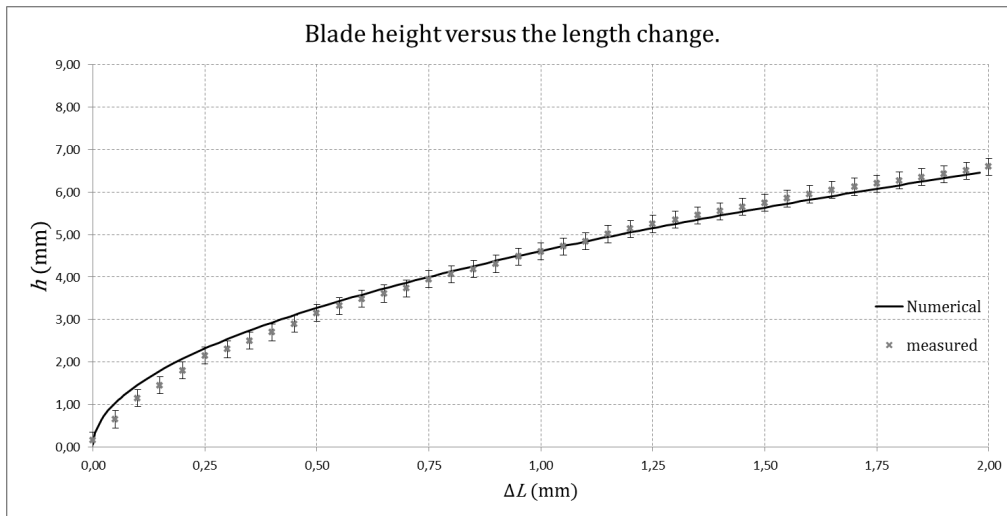


Figure 14: Numerical height of the center of the blade versus the x-displacement.

Now the numerical analysis calculation can be compared with the measurements. The accuracy of the measured points do not overlap the numerical points at the beginning, but eventually the points do overlap. This inaccuracy arise from a little offset of the experimental setup. This can be explained by some external forces and resistances in the setup. The inaccuracy is not of great importance because at the end, the analysis will be used to verify the measurements in general. Also the blades will mostly not brake between the 0 and 0.25 mm.

4 Experimental setup

A experimental setup will be discussed to understand the measurement of the bending stress . The setup is designed by Mr. Doets and a schematic reproduction is displayed in figure 15.

1. Bottom plate
2. Bracket
3. Fork 1
4. Fork 2
5. As
6. Clamp
7. Perspex block
8. Saddle
9. Saddle block
10. Extender
11. Ball Bearing
12. Load Sensor
13. Linear table

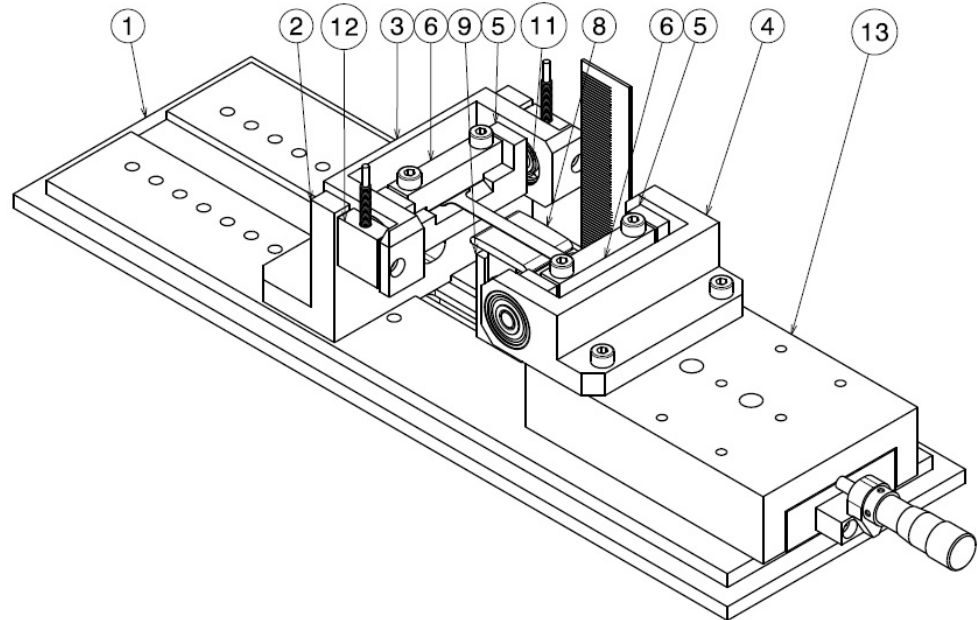


Figure 15: Schematic reproduction of the experimental setup.

A experimental setup is constructed at the Nikhef by Michiel Jaspers. As shown in figure 15, a linear mover can vary the distance between the two forks. If the forks are getting closer to each other, the silicon blade in between the forks will bend. The clamps can rotate without friction. The curvature at the center of the blade will be proportional to the distance between the two forks. Also the height at the center of the blade will be higher if the forks are getting closer to each other. The stress can be calculated with the measured height at the center of the blade and the force.

The force will be measured with load sensors as shown in figure 15. These sensors will measure a voltage. The computer will read the voltages with a data acquisition device. The data will be processed using the software of National instruments, LabVIEW. Now, the voltages can be converted to a weight and eventually to a force.

Two rotating sensors are mounted at the bottom of the clamps. These sensors are not illustrated in 15. These rotate sensors will measure the tilt of the clamps. The stress can also be calculated with the clamp rotation and the E-modulus.

The stress can be calculated using the height of the bending blade. The height of the blade will be measured using a camera and a ruler. Every step of ΔL a picture will be taken. The picture which is taken one step before the blade breaks will be used to calculate the stress. In figure 16 a picture taken with the used camera is shown.

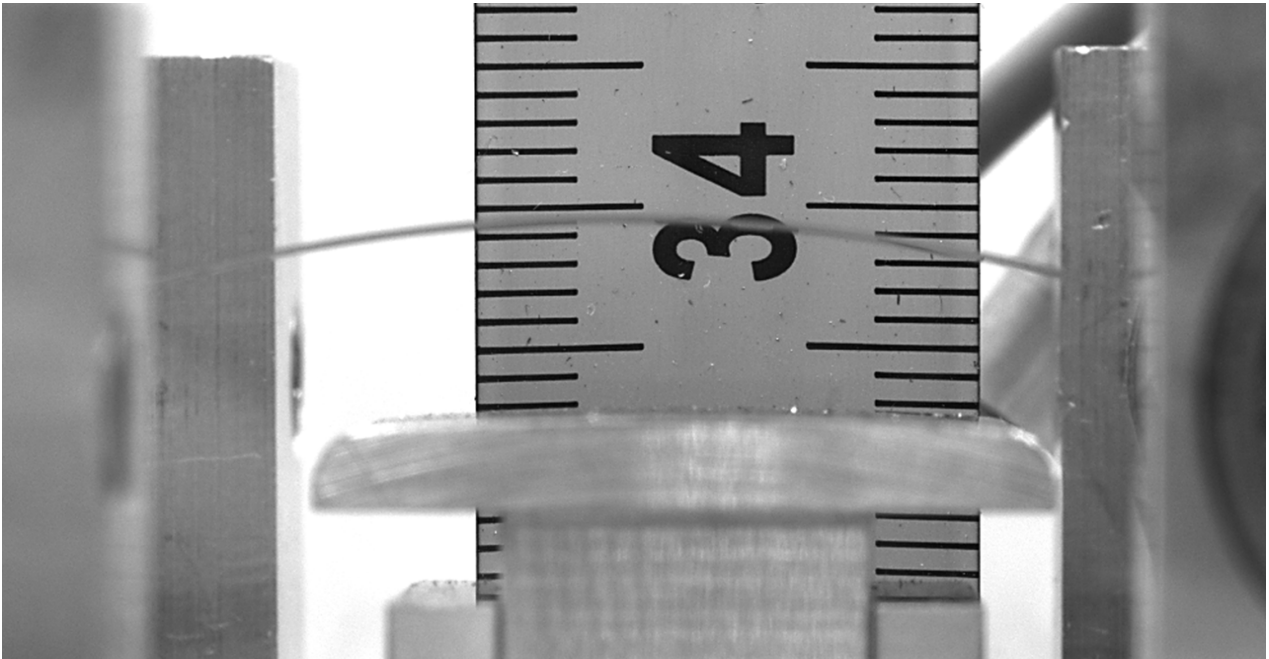


Figure 16: Picture of the height measurement.

The difference between the starting height (when the blade is flat) and the ending height (when the blade almost breaks) will be measured. Now, the height can be read of the ruler with a accuracy of 0.1 mm. Only the height at the center of the blade will be measured. This is the point where the biggest stress is applied and this is also the highest point of the blade.

4.1 Calibration of the rotation sensor

The rotation sensor needs to be calibrated before the rotation can be measured. A rotation sensor is attached on both clamps. This sensor gives a voltage of 2.5 V when the angle is 0° and 0.5 V or 4.5 V when the angle is ±90°. The angle is proportional to:

$$\theta = \arcsin\left(\frac{V_{measured} - V_{offset}}{V_{total}}\right) \quad (56)$$

where:

θ = the angle	[rad]
$V_{measured}$ = the measured voltage	[V]
V_{offset} = the offset voltage	[V]
V_{total} = the maximum voltage	[5 V]
$V_{amplitude}$ = amplitude voltage	[0.4 V]

The offset of rotation sensor 1 is estimated to be 0.50 V and the offset of rotation sensor 2 is 0.53 V. This offset is used to make the offset of both sensors the same. Now the offset point of both rotation sensors are approximately the same.

A camera is used to read the angle analog of the protractor. In figure 17 a picture of the measurement is shown. When the angle is 0° the right side of the stick designates 90°. The difference between the 90° and the designated angle is the analog measured angle. The angles measured with the angle sensors (which is called the measured angle) are plotted together with the analog angles to observe the difference. This is shown in figure 18. The gradient of the analog angle is a bit steeper than the measured angle. Also the offset of the measured angle is not zero. The difference between the average angle and the analog angle is used for the correction.

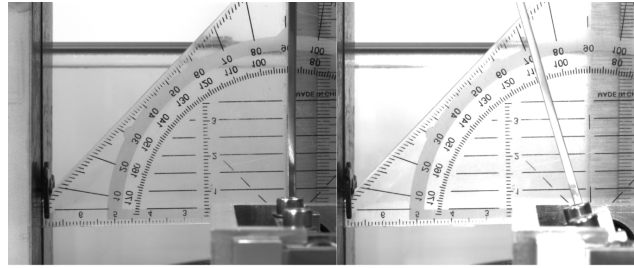


Figure 17: Picture of the analog angle measurements. left: the angle is 0° and right the angle is 19.5°.

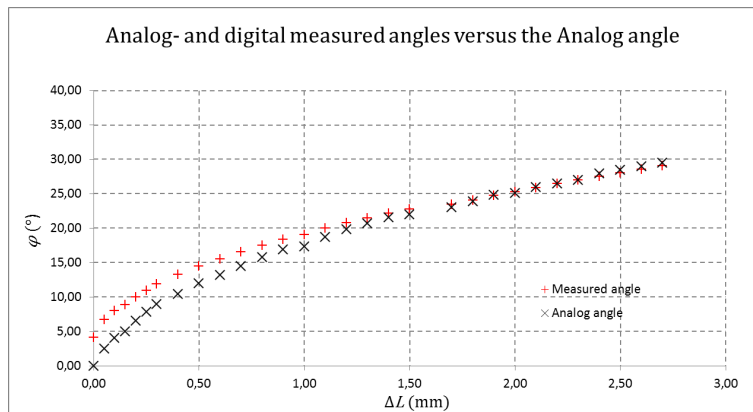


Figure 18: Measured rotations versus the Analog angle.

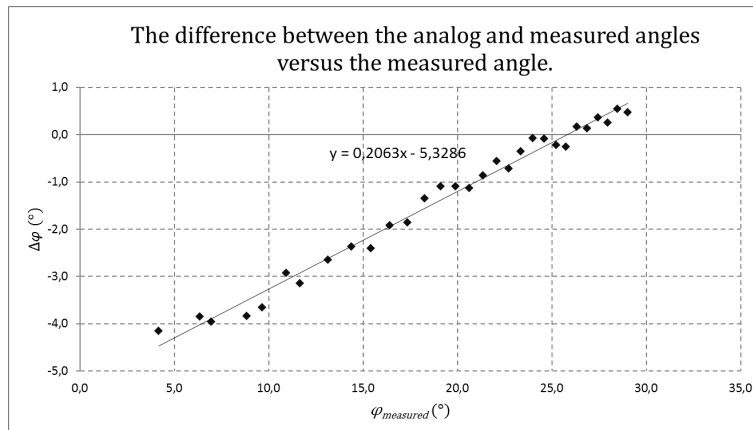


Figure 19: Angle difference between the average and analog curve

If a linear trend line is plotted through the points of difference, figure 19 arises. The difference between the measured angles and analog angles gets bigger as a function of the measured angle. The measured angle can be corrected using the gradient of the trend line in figure 19. The Gradient of

the angle differences versus the analog angles is measured 5 times and the offset of every plot are shown in table 2.

Table 2: The gradient and offset of every measurement.

Measurement	Gradient ± 0.04	Offset ± 2
1	0.21	5
2	0.21	5
3	0.21	6
4	0.17	4
5	0.17	4
Average	0.19	5

The analog angle will be estimated most reliable. The error of the measured angle can now be corrected as a function of the measured angle itself with equation:

$$\varphi_{corrected} = \varphi_{measured} - (\varphi_{measured} \cdot 0.19') - O \quad (57)$$

where:

$\varphi_{corrected}$ = the corrected angle [°]
 $\varphi_{measured}$ = the measured angle [°]
 O = the offset of the angle sensor [-]

The average gradient = 0.19 and is used for correcting the error between the measured angle and the analog angle. Now, the difference between the corrected angle and the analog angle versus the measured angle is shown in figure 20.

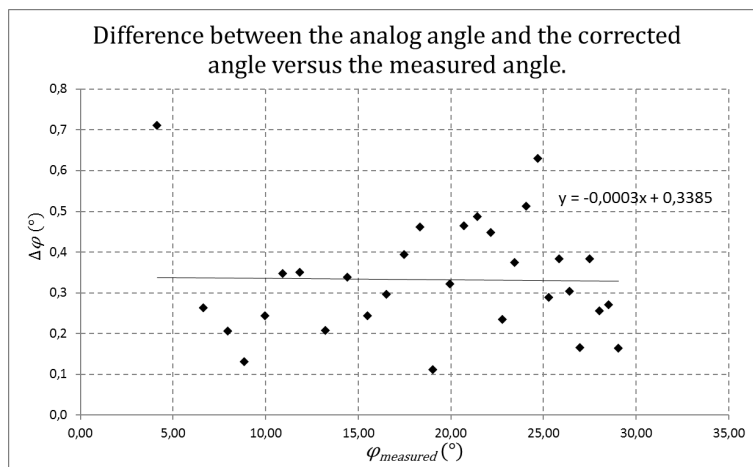


Figure 20: Angle difference between the average and analog curve.

The differences of the corrected angles are a lot smaller compared with the measured angles. Also the gradient goes to zero, which means that the relative error no longer depends on the size of the measured angle. The standard deviation σ of these errors is 0.2° . This means that the measurements have a accuracy of $3 \cdot \sigma = 0.6^\circ$.

4.2 Calibration of the load sensors.

The load sensors are mounted between the fork and the bracket as shown in figure 15. The experimental setup needs to be tilted 90° as shown in figure 21. This is because normally the load sensors are sensitive in the horizontal direction. Now the load sensors can be used in the vertical direction. The small offset of this sensor will be estimated to be the weight of the used rope and the fork.

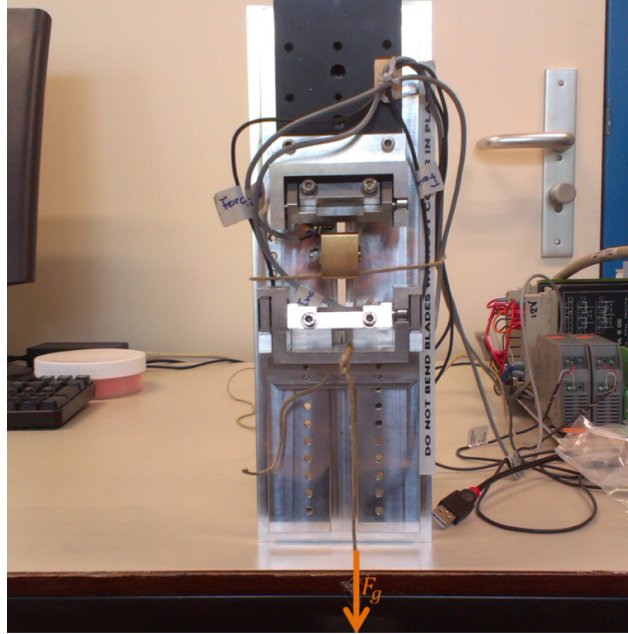


Figure 21: Load sensor calibration setup.

The range of each load sensor is between the 0 and 10 lb, which is the same as 4,54 kg. The output of the load sensor is a voltage. This voltage will be converted to a weight in the data acquisition device of National Instruments and this weight will eventually be converted to a force in the software of LabVIEW. This will be done using the equation:

$$F = mg \quad (58)$$

where:

F = the force

[N]

m = the measured weight

[kg]

g = the gravitational acceleration

[m/s²]

Variable weights are used for correction of the load sensors. A bottle with a variable volume of water is used as different weights. Every different volume is measured using a scale. The weight that the scale indicates is directly the base for the weight the load sensors needs to indicate. Different weights are measured and the difference between the measured weight with the load sensors and scale is given in figure 22.

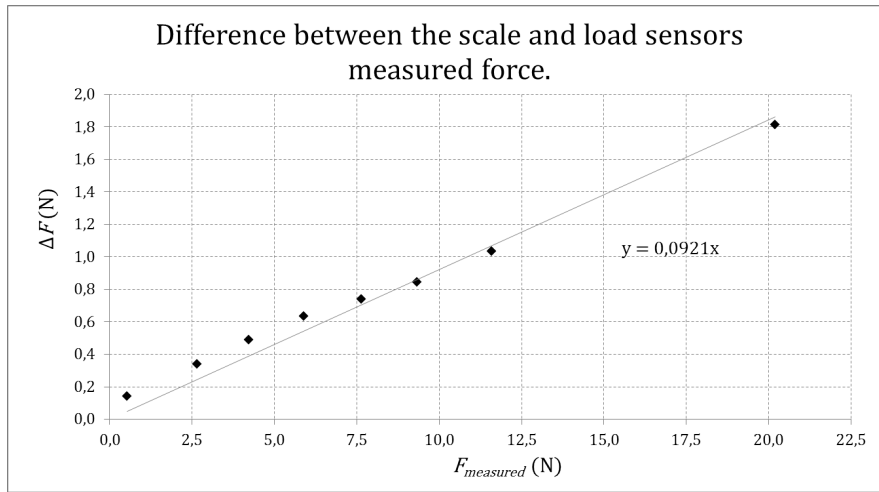


Figure 22: Difference between the scale indication and the load sensors measured force.

The difference between the scale and the load sensors will rise after the applied force rises. In this case the gradient is 0.092. Several measurements are achieved and the gradients of this measurements are shown in table 3

Table 3: Gradients at every measurement.

Measurement	Gradient ± 0.03
1	0.11
2	0.09
3	0.06
4	0.13
5	0.13
6	0.16
7	0.11
Average	0.11

This difference can be corrected as a function of the measured force with equation:

$$F_{corrected} = F_{measured} - (F_{measured} \cdot 0.11) \quad (59)$$

where:

$F_{corrected}$ = the corrected force [N]

$F_{measured}$ = the measured force [N]

ΔF = difference between measured force and the the scale indication [N]

Where $d\Delta F'$ is the average gradient of figure 22. Now, the difference between the corrected force versus the scale force is given by figure 23.

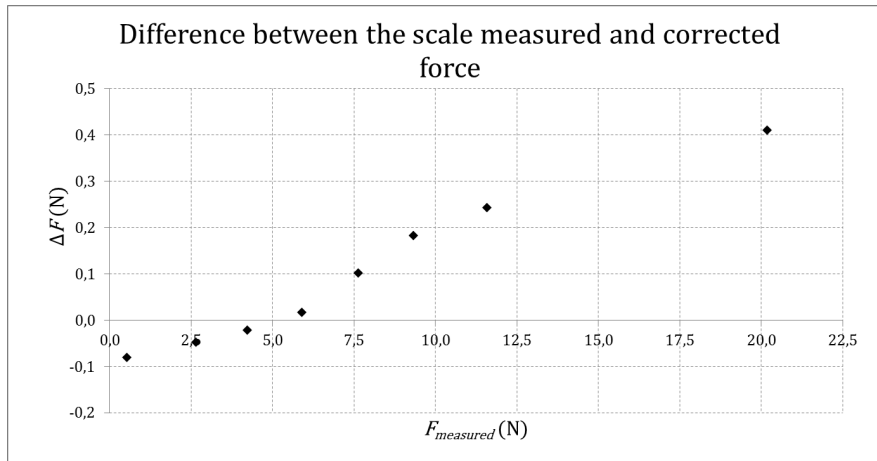


Figure 23: Difference between the scale indication and the corrected force.

Shown in figure 23 the difference between the force measured on a scale and the corrected force is much lower. The standard deviation σ of the difference is: 0.15. This means the force can be measured with a accuracy of $3 \cdot \sigma = 0.45$ N. The accuracy still get worse after the the force increases. But because the work domain of this project is between the 0 and 6 N, the deviation will not be higher than 0.1.

5 Stress measurement results

In this chapter, the measurements will be discussed. First silicon cantilever blades are measured which are hand-cut, than the machine-cut silicon blades, high energy etched blades and the chemical etched blades will be discussed. The maximum stress can be calculated with equation 16:

$$\sigma_{max} = \frac{F_x h y}{I} = \frac{6 F_x h}{w t^2}$$

This equation is derived in chapter: 3.3. To calculate the accuracy of the stress, the following equation can be used:

$$\frac{\Delta \sigma_{max}}{\sigma_{max}} = \frac{\Delta F_x}{F_x} + \frac{\Delta h}{h} + \frac{\Delta w}{w} + 2 \frac{\Delta t}{t} \quad (60)$$

An example calculation gives:

$$\begin{aligned} \Delta \sigma_{max} &= \left(\frac{\Delta F_x}{F_x} + \frac{\Delta h}{h} + \frac{\Delta w}{w} + 2 \frac{\Delta t}{t} \right) \sigma_{max} = \\ & \left(\frac{0.3}{5.5} + \frac{0.1}{4.5} + \frac{5 \cdot 10^{-3}}{12} + \frac{5 \cdot 10^{-4}}{0.2} \right) \sigma_{max} = 0.08 \cdot \sigma_{max} \end{aligned} \quad (61)$$

5.1 Hand-cut blades

The hand-cut blades are made, using a diamond-knife to apply a incision on the surface of the silicon wafer. This way a small stress potential is applied on the surface. Now, the blade will break parallel to the incision if a force is applied. As shown in figure 24 big cracks are implemented in the edge. This will probably ensure a weak point in the cantilever.

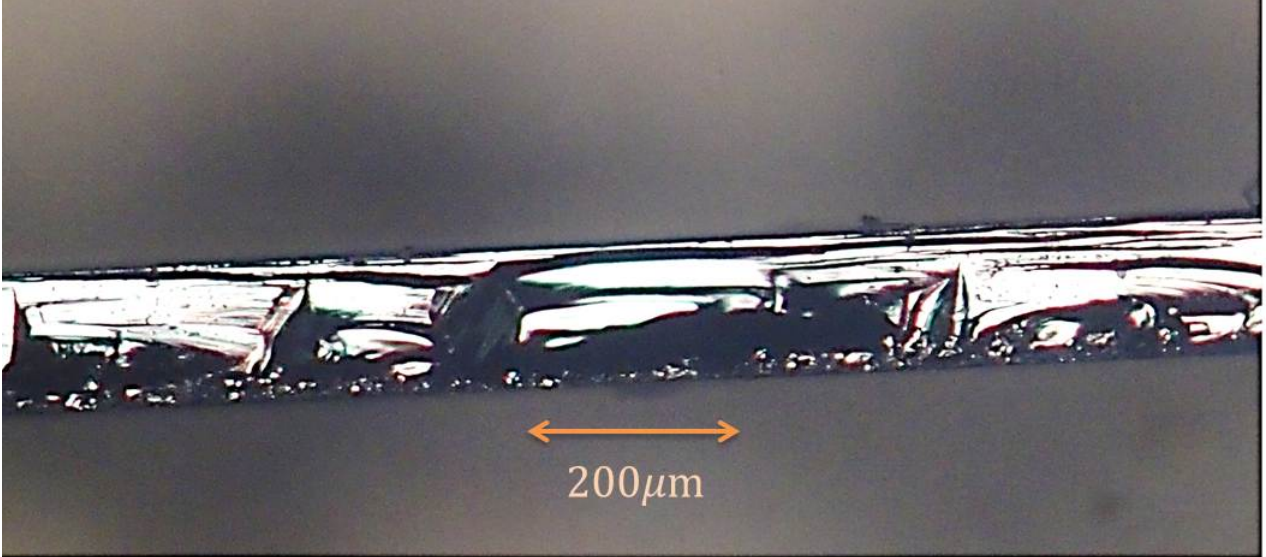


Figure 24: Silicon hand-cut blade edge.

The horizontal compression distance ΔL and the maximum stress σ_{max} is given in table 4.

Table 4: Maximum stress measurements of hand-cut cantilever blades.

Measurement	$\Delta L(mm)$ $\pm 0.005mm$	σ_{max} (MPa)
1	2.250	$(5.3 \pm 0, 5)10^2$
2	0.300	$(1.7 \pm 0.2)10^2$
3	0.400	$(1.5 \pm 0.2)10^2$
4	0.850	$(2.7 \pm 0.3)10^2$
5	1.300	$(3.3 \pm 0.3)10^2$
6	1.050	$(2.9 \pm 0.3)10^2$
7	0.750	$(2.2 \pm 0.2)10^2$
Average	0.986	$(2.8 \pm 1.3)10^2$

Because the edges are not smooth, the maximum feasible stress will differ a lot. With a standard deviation of $1.3 \cdot 10^2$ MPa, the breaking bandwidth is large. However some blade can manage high stress, the accuracy is low. This can be explained by the bad condition of the edges. This is why another solution must be considered.

5.2 Machine-cut blades

Blades can also be made using a cutting setup as shown in figure 25. This setup uses a small diamond pen to carve a small incision in the silicon wafer. Now, the place with the scratch is the weakest point and the wafer will break parallel to the scratch if a small force is applied. It is important that the scratch is made parallel to the (110)-plane. This plane is the weakest plane of the crystal structure. If a scratch is made in the (100)-plane direction, the blade will eventually also break along the (110)-plane. The scratch will be more straight and cleaner using this setup.

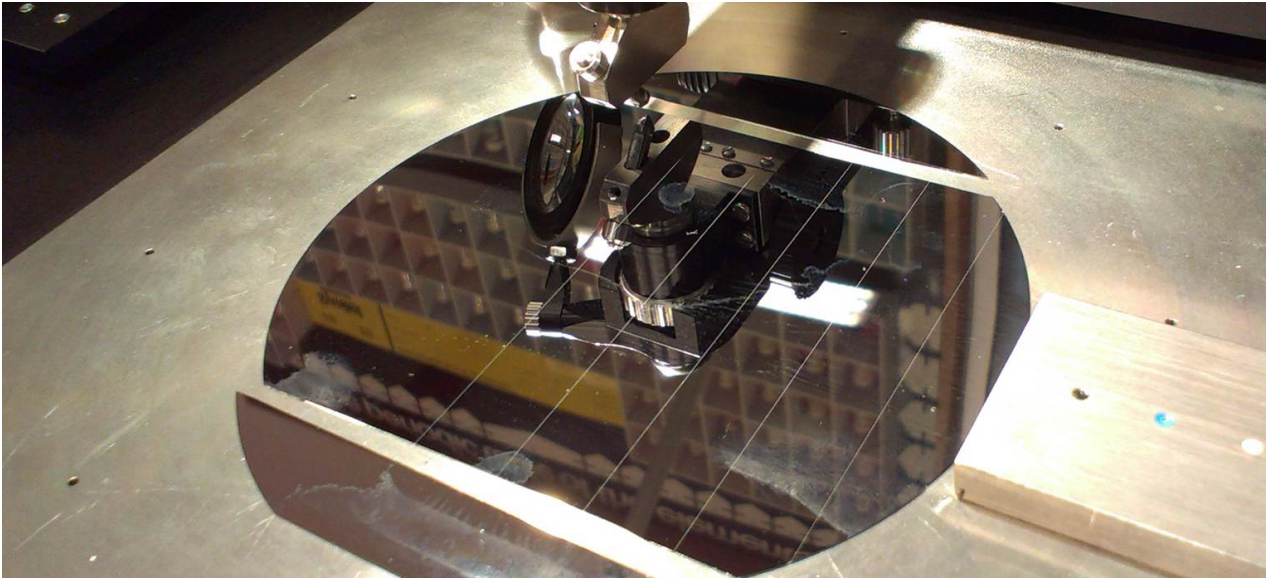


Figure 25: Image of the cutting setup.

This setup is owned by Amolf and several blades are cut out of the wafer and an image of the edge is shown in figure 26

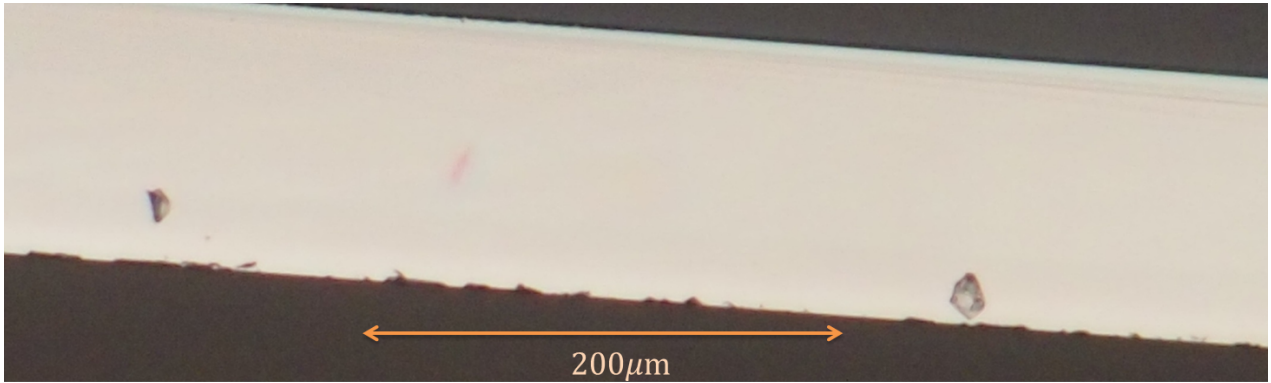


Figure 26: Image of a machine-cut blade.

As shown in figure 26, the edge is much smoother than that of the hand-cut edge. On the bottom side of the blade there are small impurities visible. These impurities are a direct result of the scratch applied with the diamond pen. If the scratch is nicely along the crystal orientation plane, the edge will be as in figure 26. How more pure and faultless the crystal-structure is, the more the blade will break along the crystal edge and without faults and cracks. The maximum feasible stress is measured and given in table 5.

Table 5: Maximum stress measurements of the machine cut cantilever blades.

Measurement	$\Delta L(mm)$ $\pm 0.005mm$	σ_{max} (MPa) straight	$\Delta L(mm)$ $\pm 0.005mm$	σ_{max} (MPa) incline
1	3.150	$(4.8 \pm 0.4)10^2$	0.250	$(1.2 \pm 0.1)10^2$
2	3.700	$(5.0 \pm 0.4)10^2$	0.400	$(1.8 \pm 0.2)10^2$
3	5.150	$(5.7 \pm 0.5)10^2$	0.650	$(2.4 \pm 0.2)10^2$
4	4.900	$(6.0 \pm 0.5)10^2$	0.850	$(2.2 \pm 0.2)10^2$
5	3.100	$(4.8 \pm 0.4)10^2$	0.850	$(2.3 \pm 0.2)10^2$
6	4.450	$(5.2 \pm 0.5)10^2$		
Average	4.075	$(5.3 \pm 0.4)10^2$	0.600	$(2.0 \pm 0.5)10^2$

The maximum feasible stress of the blades cut by the cutting setup is much higher than the hand-cut blades. However the incline cutted blades are much less strong compared with the straight cut blades. This is a direct result of the edges. The measurements shows that it is of great importance that the cut is parallel to an orientation plane. When a cut is out off the orientation plane line, the blade will break with a lot of cracks in the edge. The cutting error angle of the incline cutted blades is estimated to be 5%. With a standard deviation of 40 MPa the breaking point bandwidth of the straight cutted blades is much lower than the hand-cut blades. Also the incline cutted blades have a small breaking bandwidth with a standard deviation of 50 MPa which is a good result. In a try to improve the feasible stress of the blades, some other treatments can be performed.

5.3 Deep reactive ion etched blades (DRIE)

Most of the blades that will be measured are rectangular, only the deep ion etched blades have a special shape. A schematic design of a blade is illustrated in figure: 27. The red ends of the blade will be mounted in the clamps. This means only the small rectangular part will bend.

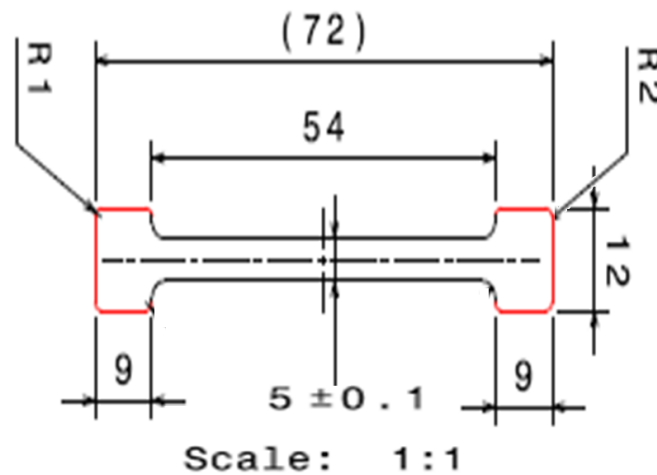


Figure 27: Design of the cantilever blade. Dimensions are in mm.

Deep ion etching is normally used for manufacturing computer chips. Material can be etched away with an accuracy of a few nanometers. It is also possible to use it for cutting the cantilever blades out of the wafer. In figure 28 the result of an ion etched cantilever is shown. The edge is much smoother than that of the hand-cut blades. Therefore a bigger magnification is used to spot the cracks in the edge. The edge is not as smooth as was hoped for because the still some cracks are visible.

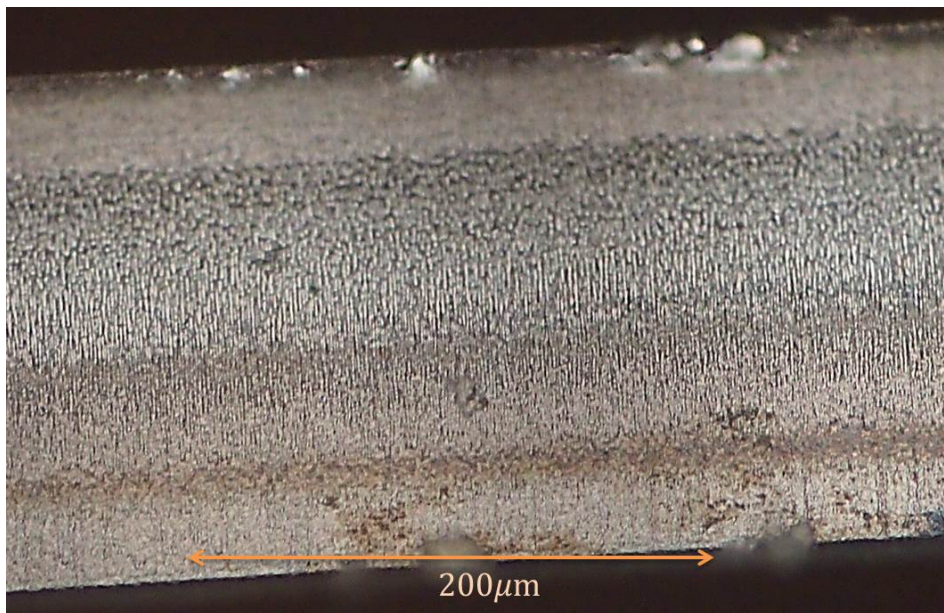


Figure 28: Silicon DRIE blade edge.

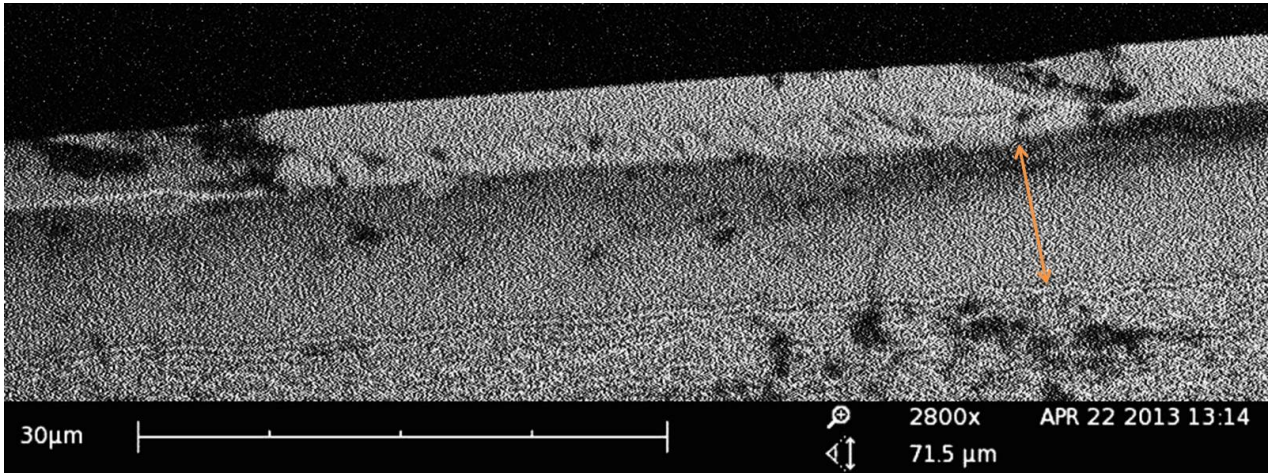


Figure 29: SEM image of an edge of a silicon cantilever.

The Deep reactive ion etched (DRIE) blades are cut using high energetic ions. These ions are shot at the surface of the blade. The interaction between the surface and the ions cause a chemical reaction. As shown in figure 29 a small gap in the edge is applied. This gap is a direct result of the ion etching method. As shown in figure 28 small impurities at the edge of the cantilever are present. This impurities can cause early breaking of the cantilever. The maximum feasible stress of these blades are measured and in table 6 the outcomes are shown.

Table 6: Maximum feasible stress measurement of the deep reactive ion etched cantilever blades.

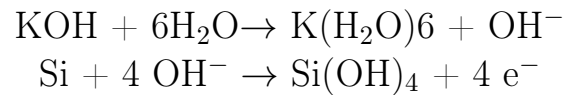
Measurement	$\Delta L(mm)$ $\pm 0.005mm$	σ_{max} (MPa)
1	0.600	$(2.2 \pm 0.2)10^2$
2	0.550	$(2.2 \pm 0.2)10^2$
3	1.100	$(3.5 \pm 0.3)10^2$
4	0.750	$(2.8 \pm 0.3)10^2$
5	0.700	$(2.5 \pm 0.2)10^2$
6	0.700	$(2.5 \pm 0.2)10^2$
7	1.200	$(3.4 \pm 0.3)10^2$
8	0.550	$(2.2 \pm 0.2)10^2$
Average	0.769	$(2.7 \pm 0.5)10^2$

The maximum feasible stress decreases compared with the straight cutted machine cut blades. With a standard deviation of: $0.5 \cdot 10^2$ MPa the breaking point bandwidth is smaller compared with the hand cut blades. It is plausible that the edges of these blades are not smooth enough. This means small cracks can simply grow during bending. A chemical etch will hopefully provide a more smoothness surface.

5.4 Chemical etched cantilevers

Chemical etching will be used to provide good bending properties. Etching is mostly used to improve the smoothness of the blade within the wafer industry. The etching is provide with a mixture of water

H₂O and potassium hydroxide (KOH). The reaction which will occur during the etching is[10]:



This chemical reaction will etch silicon of the edge. Only the edge will be on the tissue because the upper and bottom surface of the blade needs to be preserved. Figure 30 gives the experimental setup of the etching process.

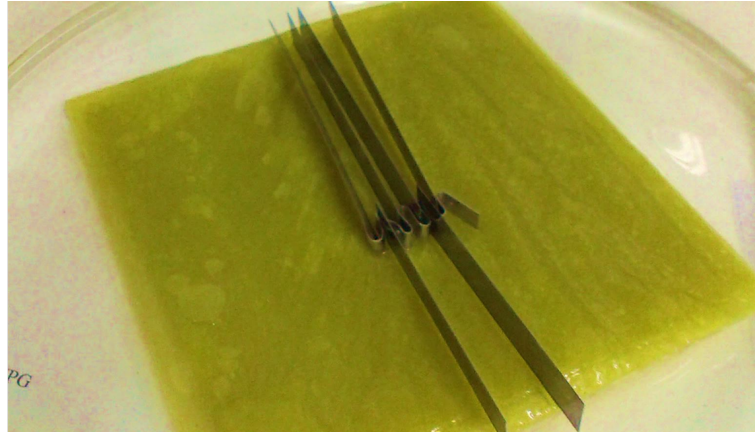


Figure 30: experimental setup of the etching process.

If the surface is in the etchant, a tarnish will occur. In figure 31 the difference between an etched and not etched edge of a cantilever is shown.

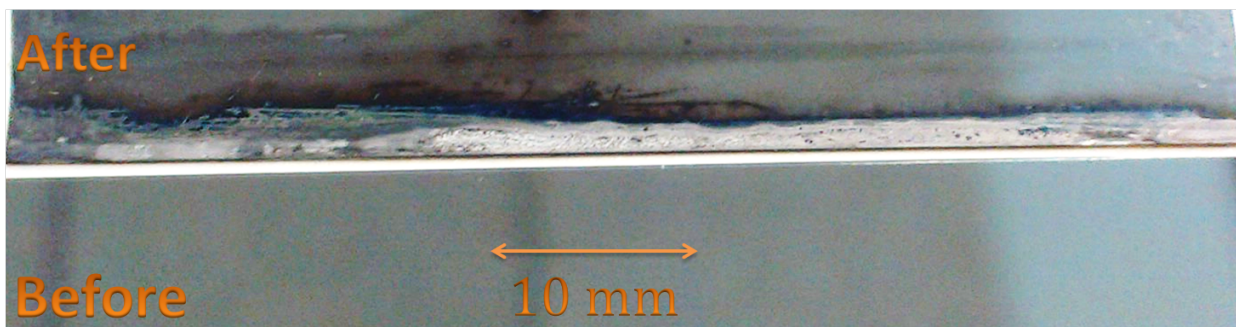


Figure 31: A before and after etching image of a silicon blade.

The time of etching will be calculated with equation 6. According to equation 6 the edge rate by 21 °C is 2 μm/h which means that the time it takes to etch 50 μm from the edge is 25 hours. To minimize the etch duration, the blade will be sandpapered before it will be chemical etched. This will decrease the big cracks and increase the smoothness. Figure 32 shows the edge of a blade which is sandpapered and chemical etched.

As shown in figure 32 the blade will not be more smooth than the machine-cut blades. The etch makes the scratches of the sandpaper smaller but at the same time impurities are made during the etching. After several blades are sandpapered and chemical etched, the measurements can be done. The measurement number, displacement ΔL and the stress σ are given in table 7:

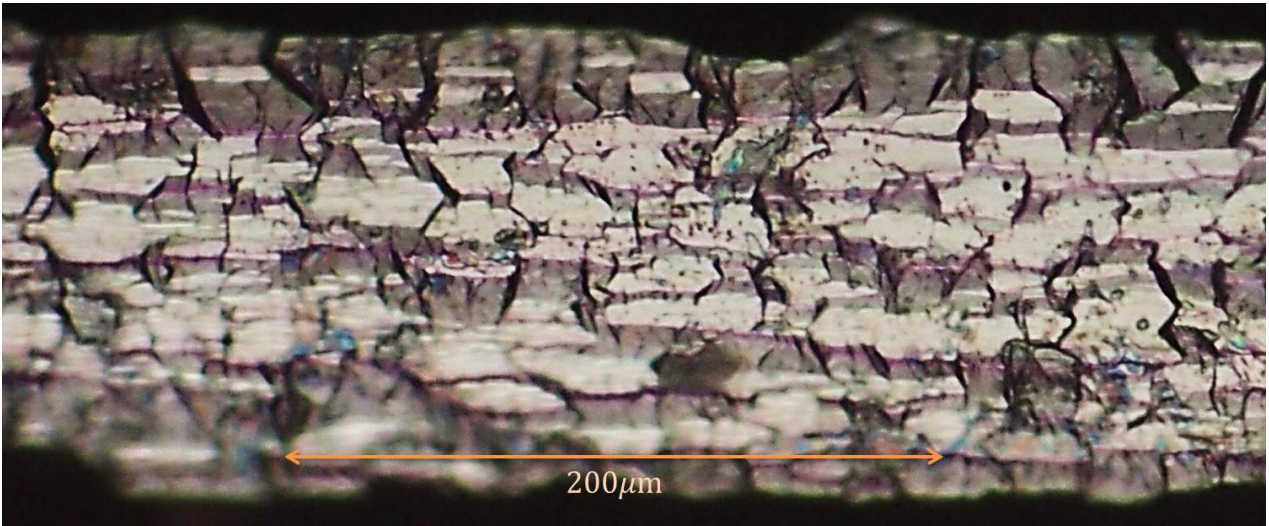


Figure 32: Image of a sandpapered and 25 hours chemical etched edge.

Table 7: Maximum stress measurements of the chemical etched cantilever blades.

Measurement	$\Delta L(mm)$ $\pm 0.005mm$	σ_{max} (MPa)
1	0.700	$(2.0 \pm 0.2)10^2$
2	0.500	$(1.9 \pm 0.2)10^2$
3	0.650	$(2.0 \pm 0.2)10^2$

During this experiment a conclusion can quickly be drawn. The feasible stress of this blades are much lower than every other setup and treatment. This can be explained by the small etch impurities on the surface of the blade. A small strip at the surface will immediately decrease the feasible stress and is not a good treatment for the blades.

6 Conclusion and discussion

During this internship a lot of silicon cantilever blades have been measured for strength. The goal was to characterize and optimize the retaining stress of cantilevers. This is performed in several ways. First silicon blades are simply cut with a diamond knife. The average feasible maximum stress of the cantilever blades is 280 MPa. The big breaking bandwidth of 130 MPa can be explained by the big cracks in the edge.

A cutting machine is also used to cut blades out of a wafer. This machine is using the same principle as the hand-cut blades only this setup is much more accurate and precise. The biggest stress can be applied if the blade is cut parallel to the (110)-orientation plane. The maximum feasible stress is much higher compared to the hand-cut blades with an average stress of 519 MPa. This blades have a small breaking bandwidth with a standard deviation of 40 MPa. The silicon prefers to break parallel to the (110)-crystal orientation but when a scratch goes a little different, the blade will be cut with a lot of cracks. This is why a cutting setup gives a better result then the hand-cut blades. The blades will break a lot faster if the blades are cut a little out of line. The average stress of the incline cutted blades is 200 MPa. Which is much lower compared to the straight cutted blades. However, a standard deviation of 50 MPa is still low compared to the hand-cut blades.

Another way to cut the cantilevers out of the wafer is using deep reactive ion etching. Using this method the edges of the cantilevers are much smoother compared to the hand-cut blades. The average maximum feasible stress is: 266 MPa. With a standard deviation of 50 MPa the breaking bandwidth is also lower than that of the hand-cut blades. However the maximum feasible stress is lower than the machine-cut blades. An explanation for this is the still the bad edge of the blades. The edge is not as bad compared with the hand-cut blades. But it is still not as smooth as wanted.

The chemical etched blades are much worse than every other setup or treatment. With a average maximum feasible stress of 200 MPa this blades will break to fast. This can be explained by the chemical impurities arising on the surface after chemical etching. Also the edge will not get smooth enough for a good result.

Some blade properties have been measured and the best result is measured by the machine-cut blades with a maximum feasible stress of 519 MPa with a deviation of 40 MPa. The blades can be made stronger using the after cut treatment: polishing. If this can be done on micron scale, the blade could manage the same stress as the machine-cut blades. Because the blades will be cut in a triangle form when used in the actual setup, the edges will not be cut along the crystal plane orientation. This is why micro-polishing will be a good alternative.

Another method which can be used is called pre-stressing. This method is mostly used in the concrete sector of buildings and bridges. Concrete is like silicon much more resistant to compression stress than tensile stress. If pre-stressing can be done with silicon, the problem of exceeding the maximum tensile stress is solved because most of the silicon will even during bending sense a compression stress instead of a tensile stress.

Also more cantilevers can be used to increase the strength. Because the mirror needs to be hanged simply more cantilevers could be used to avoid breaking. To clamp more cantilevers above each other, the lifting capacity can be increased without losing much flexibility of the cantilevers.

7 Bibliography

- [1] <http://www.ego-gw.it/public/about/welcome.aspx> (april 2013)
- [2] ET Conceptual design study, European Gravitational Observatory, Cascina, june 28, 2011
- [3] Giancoli, Physics for scientists & engineers, ISBN: 0131578499, Pearson Education, New Jersey, chapter 12.
- [4] Hopcroft, M. A. what is the Youngs modulus? Journal of microelectromechanical systems, 2010, 19, 1
- [5] Robert M.M. Mattheij, Miguel Patr  scio, Crack Propagation Analysis, TU eindhoven, report
- [6] P. Rai. Choudhury, Handbook of Microlithography, micromachining and microfabrication, Volume 2: micromachining and microfabrication, ISBN: 0819423793, Spie press, Bellingham, Washington, chapter 2.
- [7] http://www.ah-engr.com/som/10_buckling/text_10-1.htm (april 2013)
- [8] van Norel, Kimmeley, Intern rapport, student Hague University, Juli 2011.
- [9] http://www.engineersedge.com/manufacturing_spec/average_properties_structural_materials.htm (may 2013)
- [10] <http://www.allreactions.com/index.php/group-1a/potassium-k/potassium-hydroxide-koh> (april 2013)
- [11] <https://www.nikhef.nl/wetenschap-techniek/technische-afdelingen/mechanische-technologie/> (februari 2013)

A Werkplan

Tijdens het afstuderen is het de bedoeling dat een werkplan wordt opgezet. Dit werkplan heeft betrekking op de leerdoelen, planning, taken en deadlines van de afstudeerperiode in het voorjaar van 2013. De afstudeerperiode is het laatste onderdeel (in het curriculum) van de opleiding technische natuurkunde aan de Haagse Hogeschool te Delft.

Het Nikhef

"De missie van het Nationaal instituut voor subatomaire fysica Nikhef is onderzoek doen naar de interacties en structuur van de elementaire deeltjes en de krachten die er zijn op de kleinste schalen en met de hoogst haalbare energieën"[11]. Nikhef coördineert de Nederlandse experimentele activiteiten op dit gebied. Het onderzoek op Nikhef wordt gedaan voor de ontwikkeling van innovatieve technologieën. De kennis- en technologietransfer naar derden, zoals industrie, burgermaatschappij en het algemeen publiek, is een groot onderdeel van de missie van Nikhef. De afdeling mechanische Technologie ontwikkelt, ontwerpt en realiseert mechanische oplossingen voor de veelal internationale projecten waar het Nikhef aan mee werkt. De ontwikkeling van apparatuur gebeurt op Nikhef in samenwerking tussen fysici, werktuigbouwkundigen, instrumentmakers en elektronici. Hierbij wordt een groot bereik van het begrip mechanische technologie gebruikt zoals: licht en stijf construeren, vacuüm-, koel- en versnellertechniek, cryogene technieken, las- en lijmtechnieken, hoge-druktoepassingen, etc.[11].

De afstudeeropdracht

De hoofdvraag is: met welke snij toepassing en bewerking van een siliciumplaatje wordt een optimale buigstress verkregen? Om deze vraag te beantwoorden is een opstelling gebouwd waarmee een kracht in de x-richting en een hoogte van het buigpunt kan worden gemeten. Deze opstelling moet worden getest en waar nodig worden aangepast. Verwacht wordt dat de maximale stress op de siliciumplaatjes sterk afhangt van de manier hoe dit plaatje uit een wafer gesneden en bewerkt is. De plaatjes kunnen met verschillende methoden uit een wafer worden gesneden, bijvoorbeeld: snijden, laseren en draadvonken. Deze plaatjes kunnen na het snijden ook nog worden bewerkt door chemisch etsen of het polijsten van de rand. De bedoeling is om te onderzoeken wat de optimale bewerking van het plaatje is.

De toepassing

De plaatjes moeten worden gebruikt in de zwaartekrachtgolfdetector KAGRA in Japan. Deze detector wordt simpel gezegd een grote Michelson-interferometer die momenteel gebouwd wordt in Japan. De spiegels die voor de interferometer gebruikt worden zullen hangen aan draden die geen thermische energie transporteren. Omdat in de toekomst verwacht wordt dat thermische trillingen een rol gaan spelen voor de nauwkeurigheid van de metingen worden deze spiegels in een omgevingstemperatuur van 4 K gezet. Omdat de spiegels in een vacuüm staan kan de warmte van de spiegels alleen weg via de ophanging. Deze ophanging geleidt nu nog weinig tot geen warmte. Hiervoor is het onder andere de bedoeling dat de veren van silicium worden gemaakt.

B Derivation of the second moment of area

The stress cannot be measured directly. Therefore a derivation of the stress will be made. First the Force can be written as:

$$dF = \sigma dA \quad (62)$$

For the moment at point y from the neutral axis is given:

$$dM = y dF \quad (63)$$

where:

M = the moment at point y from the neutral axis [Nm]

F = force [N]

y =height from the neutral axis [m]

Combining equation 62 and 63 gives:

$$dM = y\sigma dA \quad (64)$$

The strain is given by:

$$\varepsilon = \frac{\Delta L}{L_0} = \frac{L - L_0}{L_0} = \frac{\varphi(R + y) - \varphi R}{\varphi R} = \frac{\varphi y}{\varphi R} = \frac{y}{R} \quad (65)$$

If equation 64 and 65 are combined, arises:

$$dM = E\epsilon y dA = \frac{Ey^2}{R} dA \quad (66)$$

The total moment can be obtained by integration of every small piece of surface:

$$M = \int E\epsilon y dA = \frac{E}{R} \int y^2 dA \quad (67)$$

Now, the second moment of area needs to be derived. The second moment of area is a geometrical property of a sample which describes the shape of the sample. The integral for a cantilever blade can easily be solved:

$$I_{blade} = \int y^2 dA = \int_{-\frac{t}{2}}^{\frac{t}{2}} y^2 w dy \quad (68)$$

where:

y = Height from the neutral axis [m]

w = width of the blade [m]

This makes a second moment of area of:

$$I_{blade} = \left[\frac{1}{3} y^3 w \right]_{-\frac{t}{2}}^{\frac{t}{2}} = \frac{1}{3} 2 \frac{1}{8} w t^3 = \frac{w t^3}{12} \quad (69)$$

where:

I_{blade} =second moment of area [m⁴]

t = total thickness of the blade [m]

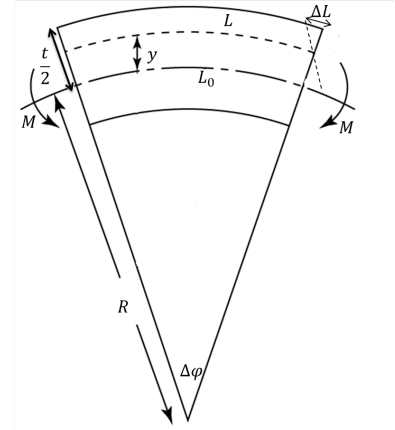


Figure 33: Schematic illustration of a small blade piece. (66)

C Derivation of the dimensionless differential equation.

The derivation of the dimensionless differential equation is given below:
Equation 41 can be written as:

$$dL = L_0 d\Gamma \quad (70)$$

Using equation 19 and 38 gives

$$\frac{Ewt^3}{12} \frac{d^2\phi}{dl^2} = -F_x z_l \quad (71)$$

Multiplying with $\frac{L_0^2}{L_0^2}$ results in:

$$\frac{d^2\phi}{dl^2} = -\frac{1}{L_0^2} \frac{12L_0^2 F_x}{Ewt^3} \sin\phi \quad (72)$$

This can be written as:

$$\frac{1}{L_0^2} \frac{d^2\phi}{d\Gamma^2} = -\frac{1}{L_0^2} G_x \sin\phi \quad (73)$$

Now the differential equation becomes:

$$\frac{d^2\phi}{d\Gamma^2} = \phi'' = -G_x \sin\phi \quad (74)$$